INL/JOU-22-67552-Revision-0

Dimensionless parameters for ballistic performance evaluation of ceramic-faced bicomponent targets against sharp-nosed projectiles

March 2023

Changing the World's Energy Future

Zherui Guo

Idaho National Laboratory

INL/JOU-22-67552-Revision-0

Dimensionless parameters for ballistic performance evaluation of ceramic-faced bicomponent targets against sharp-nosed projectiles

Zherui Guo

March 2023

Idaho National Laboratory
Idaho Falls, Idaho 83415

http://www.inl.gov

Prepared for the
U.S. Department of Energy
Under DOE Idaho Operations Office
Contract DE-AC07-05ID14517

Dimensionless parameters for ballistic performance evaluation of ceramic-faced bicomponent targets against sharp-nosed projectiles

Zherui Guo*[1]

*Corresponding author
Zherui Guo
Tel.: +1 (208) 526-3607.
E-mail address: Zherui.Guo@inl.gov
ORCiD: 0000-0002-8832-8435

[1]Idaho National Laboratory, Idaho Falls, ID, USA

*Corresponding author. Tel.: +1-(208) 526-3607. E-mail address: Zherui.Guo@INL.gov

Abstract

Two dimensionless parameters are proposed to give first-order approximations for the ballistic performance of ceramic-faced bicomponent armor plates impacted by conical-nosed steel projectiles. The current work collates expansive experimental data from Wilkins and Mayseless covering a broad range of material and mechanical properties, target construction, and projectile dimensions, the data is collapsed using the Hugoniot elastic limit of the ceramic strike face as a strength metric. Within datasets where experimental conditions are kept constant, a singular cubic curve can be generated, but variations in experimental conditions for the ballistic limit test between datasets can result in differences in the predictive curve coefficients.

Keywords: Bicomponent armor. Ballistic impact. Ceramic. Dimensionless parameters.

Introduction

Ceramics, by themselves, typically perform poorly under ballistic impact because they tend to fail catastrophically in a brittle fashion. A ductile backing material is usually used to provide adequate support to the frontal ceramic during the impact process. The hard frontal ceramic deforms and blunts the projectile, and the fracture initiation and propagation within the ceramic further dissipates the impinging kinetic energy. During this process, the ceramic fracture conoid formed helps to spread the impact load over a large area on the backing plate. Global deformation of the rear backing plate also helps to trap debris and dissipate energy, when projectile has sufficiently slowed down. This synergistic interaction between the ceramic front and ductile backing gives them the advantage of improved ballistic capabilities with reduced weight compared to monolithic metal armor systems.

Naturally, these ceramic-faced light armor systems became of interest in several scientific studies and research programs because of their effectiveness against high-velocity impact. In the 1960s, two major works by Florence and Wilkins provided robust analytical frameworks to optimize such ceramic-faced bicomponent armor systems. Florence examined the impact interaction between hard steel projectiles and lightweight composite armor systems [1,2]. In the experimental phase, hardened steel ogival projectiles were used to impact armor systems comprised of an alumina plate at the strike face bonded to fiber glass fabric or 6061-T6 aluminum alloy backing. Based on experimental results and observations, Florence derived an analytical framework to elucidate the impact mechanisms and parameters during the perforation process.

Wilkins et al. [3–7] investigated the ballistic performance of ceramic/metal composite armors via an extensive light armor program, aiming to gain in-depth fundamental insight into the perforation mechanics of lightweight composite armors through a series of experimental and numerical studies. The studies mainly looked into bicomponent armor plate systems with alumina ceramic (85% and 99% high purity) as a frontal face material backed by aluminum alloy 6061-T6 plates, but also included experimental data on alumina/fiber glass composite systems, as well as armor systems with boron carbide (B_4C) and silicon carbide (SiC) as a frontal ceramic material. Representative projectiles chosen were sharp conical-nosed and blunt flat-ended geometries. Computational simulation methods were subsequently developed based on the experimental measurements and results. The findings were concisely summarized in a later publication by Wilkins [8]. Mayseless et al. [9] further expanded the range of available ballistic data by performing essentially the same experiments as Wilkins, but with larger conical-nosed projectiles.

In the following decades, a good portion of impact research was dedicated to examining and optimizing the ceramic-faced bicomponent armor system's ballistic performance and mass efficiency. During this time, a broad body of work was either derived or improved upon from these prior studies by Florence and Wilkins. Woodward [10,11] derived a simplified one dimensional axisymmetric model based on Wilkins' experimental data. Den Reijer [12] published a thesis on theoretical and experimental work on ceramic faced armor systems, and further developed an axisymmetric target penetration model to simulate the impact mechanics.

Hetherington et al. [13,14] used Florence's analytical model to predict the ballistic performance of ceramic/glass fiber reinforced plastic (GRP) composite armor systems, and these analytical equations were further used to derive optimization curves. From this work, Wang & Lu [15] derived similar equations to investigate the effects of ceramic/aluminum thickness ratio on the bicomponent armor system's ballistic limit velocity. Zaera & Sánchez-Gálvez [16] proposed an analytical model based on a combination of Tate and Alekseevskii's model for projectile penetration into the ceramic front, and a combination of Wood and den Reijer's model for the ductile metal backing. Following this, Chocron Benloulo & Sánchez-Gálvez [17] derived a quasi-axisymmetric perforation model for ceramics backed with a fabric composite.

Moving away from specific material combinations, Ben-Dor et al. [18] returned to the analytical Florence model and derived closed-form optimization equations for arbitrary materials using their respective mechanical properties. They later improved upon these equations [19] by including the strength of the ceramic strike face, as well as an experimentally-fitted ceramic fracture conoid angle of 45° (compared to ~65° as assumed by Florence). The increased ease and lowered cost of computational simulations have also helped to provide further insight into all possible mechanisms of energy dissipation during ballistic perforation. For example, Chi & Serjouei [20–22] performed a series of experiments and simulations on ceramic/aluminum armor, and numerically obtained similar optimization curves as Ben-Dor et al. Recent studies appear to have similarly shifted towards highly compartmentalized equations for performance prediction [23,24].

The multitude of constituent material and mechanical properties as well as target structural parameters requires *a priori* knowledge of all the relevant physical quantities for performance prediction, which is not always possible to obtain. Therefore, in a departure from deriving even more overly descriptive models, we present two dimensionless parameters that provide sufficiently accurate first-order predictions for the ballistic limit of these bicomponent targets. Specifically, we focus on the interaction of sharp-nosed projectiles with ceramic-faced light armor systems.

Clearly, the efforts detailed herein are not meant to supplant other more exact methods of predicting the ballistic performance. Instead, by generalizing and parametrizing the high velocity impact response of these bicomponent target plates, we hope to provide a means for rapid deployment of similar light armor systems without necessitating all the constituent properties and structural parameters of the target plate, which may otherwise be unavailable or expensive to measure experimentally. Further, these efforts may prove useful in generating meaningful, physics-based trends for data-driven methods of performance prediction and optimization.

Dimensionless parameters for ceramic/metal bicomponent impact

The first dimensionless parameter is a ratio of the target mass to the projectile mass, given as

(1)

where A_d is the areal density of the target plate (mass per unit area), A_p is the projectile presented area, and m_p is the mass of the projectile. Cunniff previously used this dimensionless parameter to collapse ballistic impact data for fibrous soft body armor systems [25], but was later shown to arise organically in ballistic perforation models for ogival-nosed projectiles impacting monolithic metal plates [26]. Essentially, Π_1 is a geometric similarity parameter that implicitly includes the target thickness and projectile nose geometry. For a bicomponent target system, the total areal density A_d of the target plate is the sum of the constituent plates i.e.

(2)

where h_1 and h_2 are the thicknesses of the frontal ceramic and backing plate, respectively. We define two similar parameters to indicate the amount of ceramic material being used. The first parameter is k_t, given as the frontal ceramic plate thickness as a fraction of the total armor thickness

(3)

The frontal ceramic plate areal density as a fraction of the total areal density is

(4)

With either k or k_t, we can calculate an average density of the overall target plate system using a rule of mixtures. For a bicomponent system, this is given by

(5a)

This is expressed equivalently in terms of k as

(b)

The choice of k or k_t to use for trend studies is a matter of design goals. Generally, both parameters produce similar results if the material densities are not too disparate. A second dimensionless term can be formulated as

(6)

In Equation 6, V_{bl} is the ballistic limit velocity of the whole target system when impacted by some projectile, and σ is some characteristic strength term that represents the impact mechanics of the problem. For example, in a prior study by Guo & Chen investigating similar dimensionless parameters for monolithic ductile plates [27], the cavity expansion strength was used as the representative term to collapse ballistic perforation data for armor-piercing rounds, while the dynamic compressive strength was used to predict the ballistic performance of shear plug formation in ductile metal plates under FSP impact.

In the current work, the Hugoniot elastic limit is used as a characteristic strength of the bicomponent target. The Hugoniot elastic limit, or HEL, is a fundamental dynamic mechanical property describing the threshold on the material's shock Hugoniot curve at which the dynamic behavior transitions from a purely elastic state to an elastic-plastic state. While the actual HEL values are seldom directly used in the derivation of dynamics equations, prior studies have used the HEL transition point to derive other relevant physical quantities. For example, Tate suggested a linear scaling of the HEL for both the projectile and target resistance when modelling the high velocity impact penetration of long rods [28]. Rosenberg [29] related the HEL to the dynamic compressive yield strength of the ceramic. Bavdekar et al [30] demonstrated a linear relationship between the HEL and the comminuted material shear strength, and used this relationship to modify the dynamic spherical cavity expansion model for ceramics.

Results & Discussion

Due to the inherently sensitive nature of these bicomponent armor systems and their applications, complete ballistic experimental data is often scarce in literature. Existing ballistic impact studies reporting both ballistic limit velocities and the respective Hugoniot elastic limit are extremely scarce. Since ceramic properties are sensitive to their chemical composition and processing parameters, cross-referencing HEL values from other studies can often result in spurious calculations. Therefore, unless otherwise stated, data points were collated from Wilkins' experimental program on ceramic-faced armor systems [3–7] (Datasets W1–W5 in subsequent sections). Data by Mayseless et al. [9] for similar ceramic-faced bicomponent targets are also included (Dataset M). For ease of reference, material data were collated from a ceramic armor database compiled by Holmquist et al wherever possible [31], and the respective material number in the database is given where provided. In datasets W1 to W5, all projectiles were made from Allegheny steel 609 with Rockwell hardness 54–56 R_c, and have an apex cone angle of 55°. The complete raw ballistic data used in this section are given in their respective tables in the Appendix. Additional ceramic/metal impact data for alumina/Al5083 by Lee & Yoo [32] are also given in the Appendix, since the dataset was too small to provide further insight.

Dataset W1: Conical-nosed projectiles impacting AD85/Al6061-T6 targets

The conical-nosed projectiles had nominal diameters D = 6.35, 7.62, and 11.4 mm (.25-, .30, and .40-cal), and masses m_p = 4.70, 8.32, and 27.6 g respectively. Projectile velocities ranged between 200–1000 m/s. Frontal 85% purity alumina plates were manufactured by Coors (AD85). Alumina AD85 plate thicknesses h_1 ranged between 3–9 mm. Rear backing plate material was aluminum alloy 6061-T6, with density ρ_2 = 2765 kg/m^3 and plate thicknesses h_2 ranging between 3–10 mm. Frontal and backing plates were bonded using Scotchcast 221 polyurethane adhesive.

The data is collapsed onto a single curve (Figure 1) with the dimensionless parameters derived in Equations 1 and 6. For reference, the ballistic perforation results for monolithic AD85 target plates ($k = k_t = 1$ in Equation 5) are also included. A cubic curve $y = Cx^3$ was used to fit the data using the Levenberg-Marquardt algorithm.

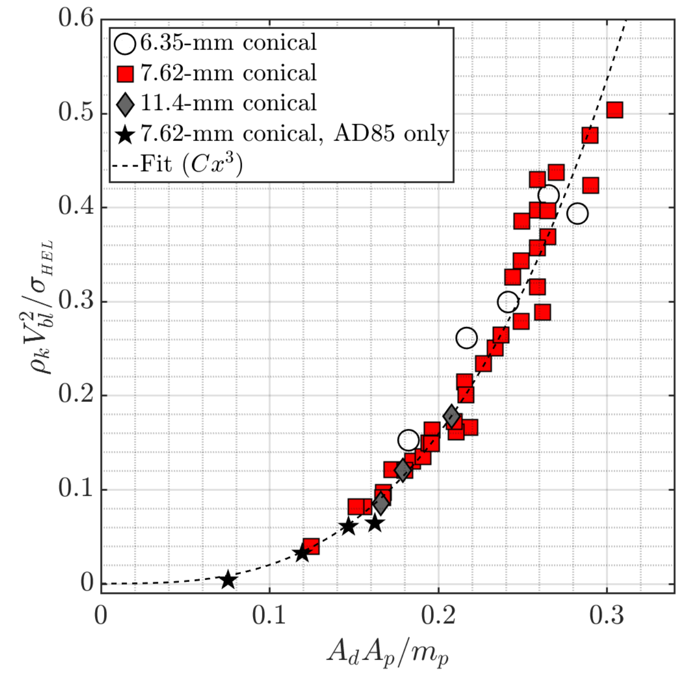

Figure 1: Conical-nosed steel projectiles of different calibers impacting AD85/Al6061-T6 targets. Fit parameters $C = 19.84$, $R^2 = 0.945$.

In this series of reports, Wilkins et al. performed dimensional scaling by using an ad-hoc factor K to normalize each projectile caliber with the 7.62-mm projectile, and the ballistic limit velocities were subsequently scaled using the term . For example, in the case of a 6.35-mm diameter projectile, the scale factor $K = 6.35/7.62 = 5/6$. In cases where the ceramic plate thickness h_1 was held constant, the scaled value was then shown to be a linear function of the backup plate thickness h_2. Without a doubt, his results show that scale factors can and do exist within the perforation mechanics of ceramic-faced bicomponent armors, but such ad-hoc scaling tends to be untenable with large datasets. On the other hand, the data lines up extremely well along a single cubic curve despite the multitude of material and geometric variables within the complex impact perforation dynamics.

Dataset W2: Conical-nosed projectiles impacting B_4C/Al6061-T6 targets

In the fourth and fifth progress reports, Wilkins reported ballistic limit velocities for frontal B_4C ceramic with Al6061 aluminum alloy backing [6,7]. Projectiles had nominal diameters $D = 6.35$, 7.62, and 11.4 mm, and respective masses $m_p = 4.70$, 8.32, and 27.6 g. Projectile velocities ranged between 500–1000 m/s. Frontal B_4C plate thicknesses h_1 ranged between 5–10 mm. Rear backing plate material was aluminum alloy 6061-T6, with density ρ_2 = 2765 kg/m^3 and plate thicknesses h_2 between 5–10 mm. Frontal and backing plates were bonded using Scotchcast 221 polyurethane adhesive.

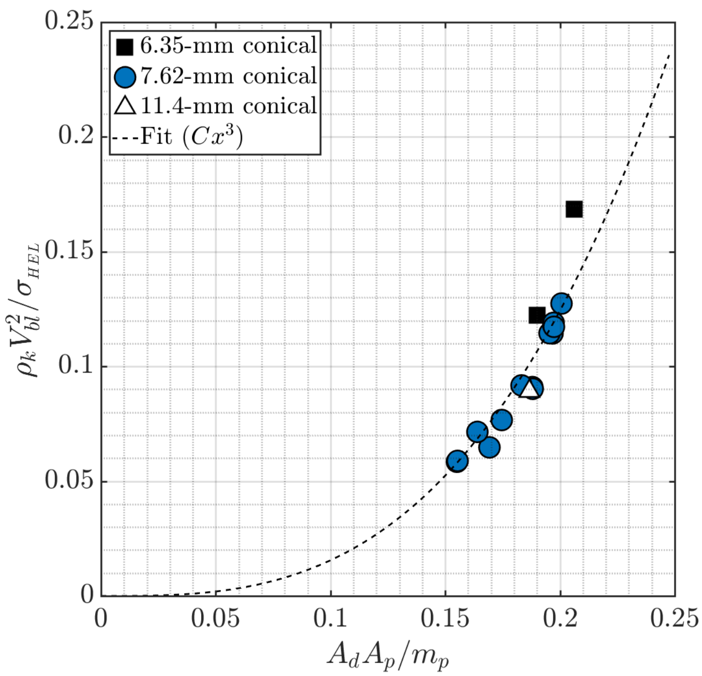

Figure 2: Conical-nosed steel projectiles of different calibers impacting B_4C/Al6061-T6 targets. Cubic fit coefficient C = 14.91, R^2 = 0.947.

Wilkins noted that the B_4C/Al6061 target system performed significantly better against the smallest 6.35-mm diameter conical-nosed projectiles, and his proposed ad-hoc scale factor was not able to account for this underprediction in V_{bl} (-14%). The dependence of the ballistic performance of B_4C on its fabrication process was given as the primary reason for such a discrepancy. Due to the different grain sizes and porosities within the B_4C ceramic resulting from these fabrication differences, a significantly increased strength and ballistic performance was observed. Likewise, the HEL differences were not accounted for in this case since a singular value of 15.0 GPa was used, thereby leading to the same underprediction in Figure 2.

This discrepancy due to incorrect material properties aside, we note that the areal density ratio parameter can effectively collapse the data regardless of the projectile caliber or target thickness regime. In both datasets W1 and W2, the collapsed dimensionless data fall along a cubic curve, and for both datasets, the backing plate was made of 6061-T6 aluminum alloy. We show the same cubic relation for a different backing material in dataset W3.

Dataset W3: Conical-nosed projectiles impacting AD85/glass fiber reinforced polymer targets

Projectiles in this dataset had nominal diameters D = 7.62 mm, and mass m_p = 8.32 g. Projectile velocities ranged between 200–1000 m/s. Alumina AD85 (manufactured by Coors) plate thicknesses h_1 ranged between 3–9 mm. Rear backing plate material was REPCO woven roving glass fiber reinforced polymer (GFRP), with density ρ_2 = 1750 kg/m^3 and laminate total thicknesses h_2 between 3–12 mm. Frontal and backing plates were bonded using Scotchcast 221 polyurethane adhesive. Ballistic perforation results for monolithic AD85 target plates are also included for reference in Figure 3.

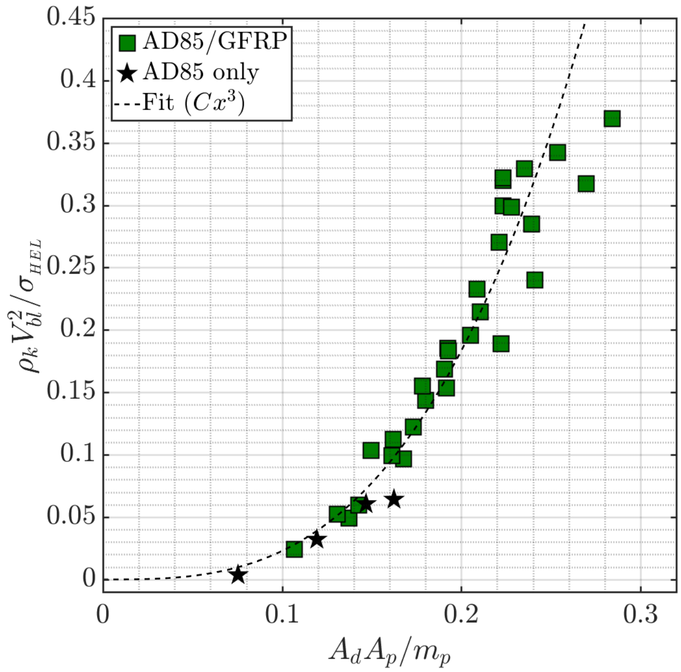

Figure 3: 7.62-mm diameter conical-nosed steel projectiles impacting AD85/GFRP targets. Fit parameters C = 22.92, R^2 = 0.995.

This cubic relation between dimensionless parameters appears generalizable to various combinations of ceramic-faced bicomponent systems, suggesting that the V_{bl} is more strongly dependent on the ceramic plate's material and mechanical properties within the regime of experimental parameters examined. This is further explored for several a broad range of backing materials with an AD85 alumina ceramic strike face.

Dataset W4: Conical-nosed projectiles impacting AD85 backed by various materials

In the third progress report, Wilkins et al. presented a dataset for 85% purity alumina (AD85, manufactured by Coors) backed with a broad variety of materials [5]. As with previous datasets, the projectiles had a nominal diameter D = 7.62 mm, and projectile mass m_p = 8.32 g. Projectile velocities ranged between 600–950 m/s. All alumina AD85 frontal plates were of thicknesses h_1 = 8.64 mm. Certain backing plates comprised two separate materials – these are considered in this study as one monolithic backing plate. Frontal and backing plates were bonded using

Scotchcast 221 polyurethane adhesive. For reference, the ballistic perforation results for monolithic AD85 target plates are also included (Figure 4).

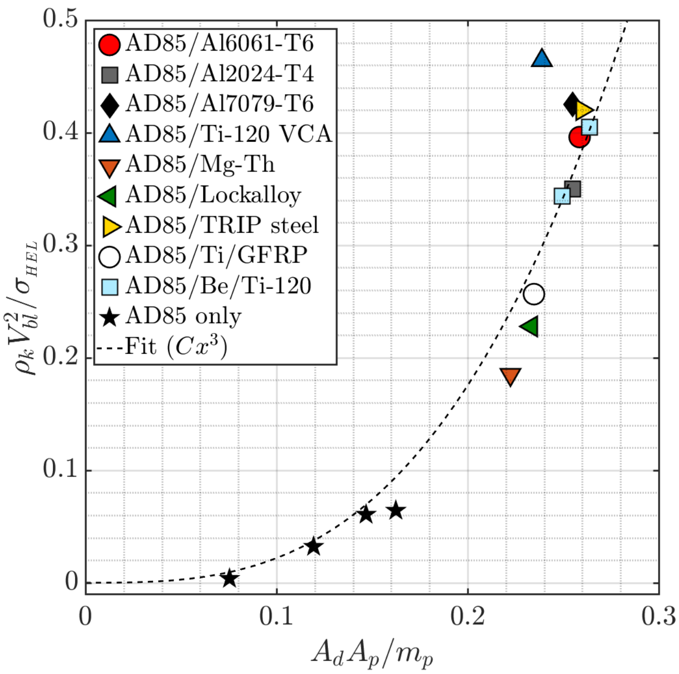

Figure 4: 7.62-mm diameter conical-nosed steel projectiles impacting AD85 alumina backed with different materials (Dataset W4). Fit parameters C = 22.09, R^2 = 0.993.

The most significant outlier is the AD85/Ti-120 VCA (Ti-13V-l1Cr-3Al) bicomponent plate, which appears to far outperform all other ceramic-front combinations for its weight. This suggests some overall synergistic structural effects due to target construction that were not explicitly examined, although the data is still well-predicted by the cubic curve for a majority of the collated data points.

Dataset W5: Conical-nosed projectiles impacting various ceramics backed by Al6061-T6

In the fourth progress report, Wilkins et al. presented a dataset for various ceramics backed by Al6061-T6 plates [6]. As with previous datasets, the projectiles had a nominal diameter D = 7.62 mm, and projectile mass m_p = 8.32 g. Projectile velocities ranged between 600–950 m/s. All Al6061-T6 backing plates were of thicknesses h_2 = 6.35 mm. Frontal and backing plates were bonded using Scotchcast 221 polyurethane adhesive.

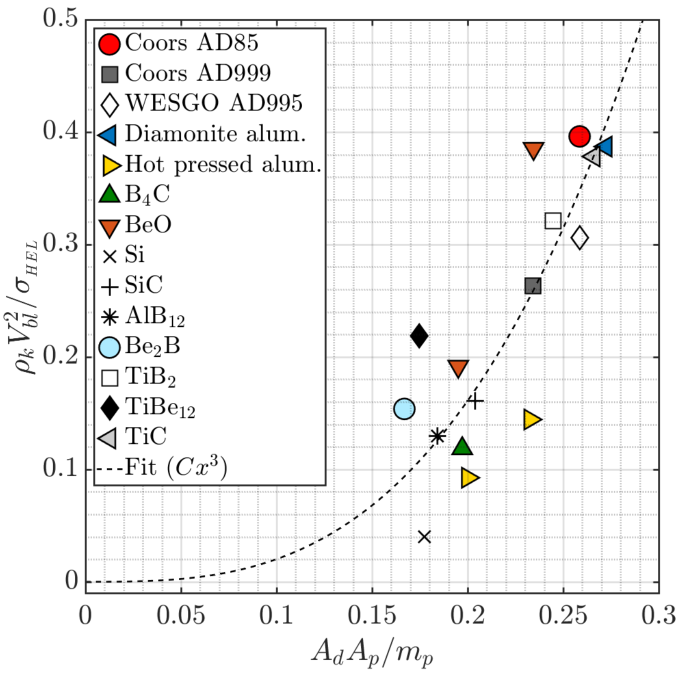

Figure 5: 7.62-mm diameter conical-nosed steel projectiles impacting various ceramic/Al6061-T6 targets. Fit parameters C = 19.57, R^2 = 0.766.

Collapsing the data (Figure 5) offers some valuable insight into the relative performance of a certain target system, i.e., how well a ceramic-faced armor target *should* theoretically perform with a certain Hugoniot elastic limit. This may be exemplified with the two data points for Carborundum hot pressed alumina/Al6061-T6 target plates with h_1 = 4.83 and 6.35 mm, h_2 = 6.35 mm, and ballistic limits of 630 and 775 m/s respectively. For a frontal ceramic HEL of 14.0 GPa, the predicted V_{bl} velocities should be 838 and 1040 m/s respectively. This likely indicates either possible underperforming or a slight difference in failure mode due to processing parameters. On the other hand, the titanium compounds TiB_2 and $TiBe_{12}$ appear to outperform similar ceramic-faced bicomponent constructions for the same weight.

Ensemble data collated from Wilkins' experiments

Despite the complex impact mechanics of ceramic-faced bicomponent target systems, Datasets W1 to W5 have shown that it may be possible to collapse their ballistic performance along a singular cubic curve for first-order predictions. Indeed, by collating ballistic data across multiple combinations of frontal ceramic and backing materials, for different target plate thicknesses, relative ceramic thicknesses, and different conical projectile calibers, the data collapses neatly along a singular cubic curve (Figure 6). Other than datasets W1 to W5, additional data points for B_4C/GFRP have also been included. By using the Hugoniot elastic limit as the characteristic strength term for all ceramics considered in this study, the ballistic performance can be reasonably predicted using a perfectly cubic curve.

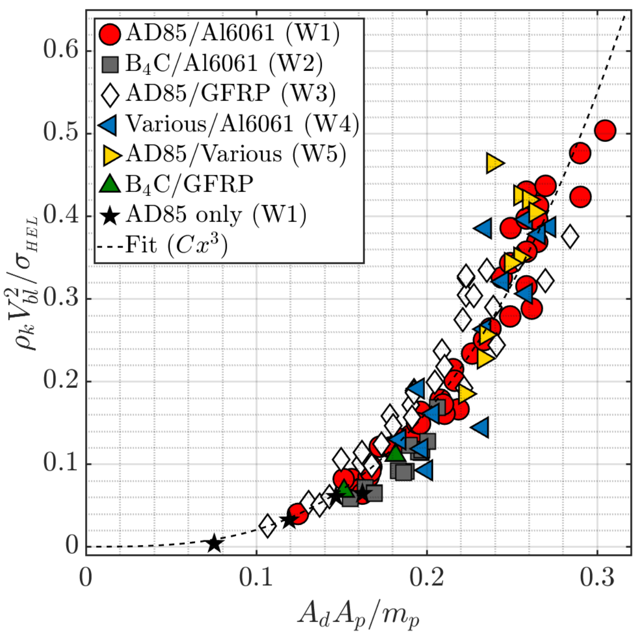

Figure 6: Ensemble of Wilkins ballistic impact data collapsed using dimensionless parameters along a cubic curve. Cubic fit coefficient C = 20.32, R^2 = 0.900.

Dataset M: Conical-nosed projectiles impacting AD85/various backing materials

The ballistic data reported by Mayseless et al were collapsed in the same fashion as the Wilkins data (Figure 7). Since no database of experimental values were available for this study, plate thicknesses and corresponding ballistic limit velocities were digitized from scanned plots in Ref. [9] and may result in slight deviations from their actual value. Compared to Wilkins, Mayseless used much larger conical-nosed projectiles of diameter D = 12.7 mm and mass m_p = 30 g [9]. The projectiles had an apex cone angle of 60° and a slightly higher Rockwell hardness of 60 R_c. Projectile velocities ranged between 100–700 m/s. Frontal AD85 alumina plates have an assumed HEL = 6.0 GPa and density ρ_1 = 3410 kg/m^3 [31], which were values previously reported by Rosenberg. The alumina AD85 plate thickness h_1 was held constant at 6.35 mm. Several materials were used for backing plates: resin-impregnated Kevlar 29 (ρ_2 = 1200 kg/m^3), aluminum alloy 6061-T6 (ρ_2 = 2700 kg/m^3), aluminum alloy 2024-O (ρ_2 = 2780 kg/m^3), mild steel alloy SAE 1020 (ρ_2 = 7870 kg/m^3), and a hardened steel alloy SAE 4130 (ρ_2 = 7850 kg/m^3). Backing plate thicknesses h_2 ranged from 3–12.7 mm. Frontal and backing plates were bonded using an unspecified adhesive.

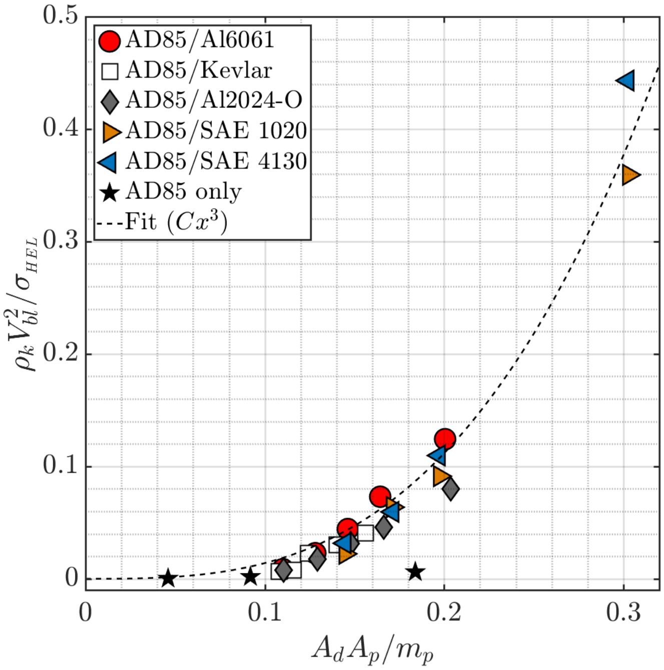

Figure 7: 12.7-mm diameter conical-nosed steel projectiles impacting AD85 alumina backed with different materials. Cubic fit parameters C = 13.95, R^2 = 0.969.

Due to the large mass of the projectile used by Mayseless et al, the collapsed ballistic data generally populates the lower regimes of mass ratios. The ceramic-faced bicomponent data still strictly follows a cubic trend regardless of backing material. The clear underperforming outlier is a 12.7-mm thick monolithic AD85 ceramic target, with an extremely low V_{bl} of 103 m/s for its areal mass. The results are qualitatively similar to Figure 6, but the Mayseless curve (C = 13.95) lies slightly below the Wilkins curve (C = 20.32). While Mayseless generally attributed this to the larger mass and the slightly higher hardness of their impinging projectile, we briefly discuss the influence of possible experimental parameters that might affect the prediction curve.

The first and biggest dissimilarity between the Wilkins and Mayseless datasets lies with the projectile physical dimensions, specifically the calibers and their corresponding masses used in each study. Mayseless described a rudimentary form of mass scaling between their data and Wilkins' data. This suggests that the areal mass ratio parameter Π_1 should sufficiently capture these mass differences between the two studies, as it did with projectiles of different calibers in datasets W1 and W2 (Figures 1 and 2). The next dissimilarity in physical geometry, though not discussed by Mayseless, is the projectile apex cone angle. Similarly, the projectile apex cone angle is implicitly included in the parameter Π_1 (Equation 1). Moreover, the slight difference in cone angle (55° vs. 60°) is unlikely to have such a significant effect.

The next consideration is the difference in projectile hardness (54–56 vs. 60 R_c for Wilkins and Mayseless, respectively). As Wilkins briefly discussed in the final report [7], projectile strength effects dominate in impact scenarios where the projectile is much stronger than the target. Conversely, when the target material is stronger than the impinging projectile, the perforation process is mostly governed by the projectile mass and striking velocity. In the case of all of Wilkins' datasets W1 to W5, the steel projectile is considerably weaker than the strike face ceramics tested, which explains why the ballistic performance can be collapsed using only the projectile mass and velocity. Although the effects of projectile strength were qualitatively discussed in terms of their respective ballistic limit velocities, Wilkins did not give a quantitative comparison of projectile material strengths relative to the target ceramic material. Relating the projectile hardness to the ballistic performance necessitates a discussion of the projectile failure mode, and such an effort is qualitative at best without strength metrics. Regardless, even though such relative strength effects should be further studied and quantified, it is somewhat unlikely in this case that such a minute difference in projectile hardness would constitute a significant change in ballistic performance.

An oft-overlooked factor when comparing ballistic data across different ceramic plate perforation studies is the difference in target mounting methods. In Wilkins' experiments, the target plates of dimensions 152 mm ×152 mm were clamped at the corners; in Mayseless' experiments, circular alumina plates of diameter 130 mm were fixed to backing plates of diameter 140 mm. The bicomponent target plates were clamped around the entire circumference with clamping diameter 114 mm. Clearly, in a high velocity impact scenario where mechanical waves (e.g., transverse shear, dilatational, flexural) are propagating at varying timescales from the point of impact, boundary conditions have to play a role in the local and global deformation of the target. The influence of experimental setup on the measured ballistic performance has been well-documented in a prior literature review by Walley [33]. Likely, the difference in the Wilkins and Mayseless datasets are a result of a combination of these individual factors, some more so than others. Nonetheless, within the same study and all other conditions held constant, the data points are collapsed along a cubic curve as well.

Limitations of current datasets

The data examined thus far agree with Wilkins' observations that, for the same backing material the whole target perforation process is mostly governed by the projectile mass and striking velocity when the ceramic material is stronger than the impinging projectile. For such a projectile-target interaction, the collapsed experimental data can be grouped along a single cubic curve as demonstrated when applying the same dimensionless parameters to the Mayseless dataset. The results are generally surprising, considering that the prediction curve was formulated only with rudimentary mass and kinetic energy terms regardless of the relevant material and mechanical properties of the backing. In other words, for the datasets discussed herein, the bicomponent target performance is *mainly* dominated by the ballistic impact response and interaction of the frontal ceramic and the steel projectile, while the rear plate contributes through its areal mass within the regime of experimental parameters examined in this work.

Collapsing the experimental ballistic perforation data for a broad range of materials allows us to perform parametric scaling based on the similarities in the entire impact phenomena. In other words, for some sharp projectile impacting some arbitrary bicomponent target plate with a stronger frontal ceramic material than the projectile material, the initiated ballistic impact responses are similar, and the ballistic limit data points will lie on the same cubic curve. In the present discussion, the failure modes of either the ceramic, backing, or projectile have not been explicitly considered. The results from the current work seem to imply that certain strength-dependent mechanics of ballistic perforation can be considered somewhat negligible within the regime of examined structural parameters. While these other effects may contribute to the overall ballistic performance, their respective order of magnitude may not be as large as the dependence on the dynamic failure strength of the ceramic.

Such an assumption clearly will not hold across all projectile/target material pairs, as evidenced by Wilkins' dataset for projectile materials of different strengths impacting AD85/Al6061-T6 plates [6]. Additionally, in the case of B_4C/Al6061-T6 and the Mayseless datasets, some sort of difference in ballistic response or component failure modes must be addressed. Likely, the effects of the relative strengths result in a slightly different failure mode and impact response, and manifest themselves in the cubic coefficient C term. More ballistic limit velocity data for different projectile materials would reveal more predictive trends.

Further discussion

In a previous work by Rosenberg & Yeshurun, the ballistic limit velocities for several ceramics (some of which are included in Figure 5) were shown to fall on a single curve that decreases with increasing density [34]. This was attributed to the differences in ceramic thicknesses in order to achieve the same areal densities of the final bicomponent products. For the same ceramic areal density, a less dense ceramic will be thicker and vice versa, and this larger thickness leads to longer dwell times before complete ceramic failure, which consequently results in a better ceramic performance. In the V_{bl} plate perforation test, these interdependent effects are difficult to isolate.

To circumvent these problems related to plate perforation tests, a thick-backing technique was developed to isolate the effects of compressive strength during ballistic impact by eliminating two main issues with the V_{bl} test configuration: the influence of the backing material, and the tensile bending stresses on the rear free surface [35]. With this proposed testing configuration (termed the depth of penetration test, or DOP), a standardized method was developed to rank the relative performance of these different ceramics via an ad-hoc dimensionless ballistic efficiency metric

(7)

where P_{ref} is the reference penetration depth of a projectile penetrating a thick monolithic backing block (usually aluminum) at some impact velocity, P_{res} is the residual penetration depth of the block with a ceramic tile front, $\rho_c h_c$ is the areal density of the ceramic tile, and is the minimum ceramic thickness for zero residual penetration. This ballistic efficiency metric has proven extremely effective for materials selection in the design of armor systems via an objective, test-independent criterion.

The DOP test configuration provides an objective measure of the ceramic tile's ballistic efficiency without the influence of any complicating factors. On the other hand, the V_{bl} test provides a direct, quantitative measure of the ballistic performance of a target plate system configuration under deployment against a specific projectile threat. In other words, the ballistic limit V_{bl} measured is a function of all the parameters involved in the construction of the target plate as necessary to defeat a particular high velocity impinging projectile. Since Equation 7 does not explicitly contain a ballistic limit velocity, it can be difficult or near impossible to back out a direct quantitative measure of the target plate performance without *a priori* knowledge of the reference DOP test parameters such as impact velocity and reference penetration depth. Conversely, the performance of a particular plate construction against a specific ballistic threat can be approximated using known material properties via the proposed dimensionless parameters in this work.

Although Rosenberg's study claimed to have collated Wilkins' experimental data for several ceramics with equal areal density backed by a 6.35-mm thick Al6061 rear plate, we were unable to find the same experimental data points that were used to demonstrate the inverse relation to the frontal ceramic density. We further discuss this in the Appendix. Nonetheless, we used our collated experimental dataset for all ceramics backed with a 6.35-mm thick Al6061 rear plate (Table I). Note that the Spearman correlation coefficient is used here instead of the usual R^2 coefficient, since the relations between variables are monotonic, but not necessarily linear. Clearly, the ballistic limit velocity V_{bl} as a standalone metric is only weakly dependent on the ceramic Hugoniot elastic limit strength value. However, if the V_{bl} is normalized with respect to the ceramic areal density to account for the combined effects of the ceramic thickness and density, the HEL becomes a stronger influencing factor in the final performance prediction.

Table I: Spearman's correlation coefficient ρ values of various factors collated from Wilkins' data.

Variable 1	**Variable 2**	**Spearman's ρ**
h_1	V_{bl}	0.90
ρ_1	V_{bl}	-0.02
$A_{d,1}$	V_{bl}	0.47
HEL	V_{bl}	0.11
HEL	V_{bl}/ρ_1	0.67
HEL	$V_{bl}/A_{d,1}$	0.71

Rosenberg et al. discussed the dependence of η on both the density and strength of the ceramic tile [36], a conclusion that is also highlighted in this current work, albeit in a different form. Specifically, in their work, a comparison was drawn between two alumina ceramics, AD85 and BC90G, and their resultant ballistic efficiency metrics η were related qualitatively to their respective Hugoniot elastic limits. As such, the parametrization efforts detailed herein are complementary to their work. It may even be possible to unify the dimensionless parameters along with the ballistic efficiency metric for rapid design and deployment of ceramic-faced bicomponent systems.

Conclusions

Two dimensionless parameters are shown to collapse the experimental ballistic data for a broad range of material and mechanical properties, target structural parameters, and projectile dimensions along a singular curve. The Hugoniot elastic limit of the ceramic strike face was used as a strength metric for dimensionless parametrization. The results suggest that, for projectile/target pairs exhibiting similar overall ballistic impact response, the complex high-velocity perforation mechanics of such ceramic-faced bicomponent systems can be sufficiently described using the two dimensionless parameters. The first-order approximations provided by the current work will provide a means for rapid deployment of similar light armor systems without necessitating the constituent properties and structural parameters of the target plate, which may otherwise be unavailable. These efforts may further prove useful for future data-driven methods of performance prediction and optimization.

Declaration of Competing Interest

The author declares no known competing financial interests or personal relationships in the publication of this paper.

Acknowledgments

Work was supported through the INL Laboratory Directed Research & Development (LDRD) Program under DOE Idaho Operations Office Contract DE-AC07-05ID14517.

References

[1] A.L. Florence, T.J. Ahrens, Interaction of projectiles and composite armor (AMRA CR 67-05F), 1967.

[2] A.L. Florence, Interaction of Projectiles and Composite Armor Part II (AMMRC CR 69-15), 1969.

[3] M. Wilkins, C. Honodel, D. Sawle, An Approach to the Study of Light Armor (UCRL-50284), Livermore, CA, 1967.

[4] M.L. Wilkins, Second Progress Report of Light Armor Program (UCRL-50349), 1967.

[5] M.L. Wilkins, Third Progress Report of Light Armor Program (UCRL-50460), Livermore, CA, 1968.

[6] M.L. Wilkins, C.F. Cline, C.A. Honodel, Fourth progress report of light armor program (UCRL-50694), (1969) 56. doi:10.2172/4173151.

[7] M.L. Wilkins, R.L. Landingham, C.A. Honodel, Fifth Progress Report of Light Armor Program (UCRL-50980), 1970.

[8] M.L. Wilkins, Mechanics of penetration and perforation, Int. J. Eng. Sci. 16 (1978) 793–807. doi:10.1016/0020-7225(78)90066-6.

[9] M. Mayseless, W. Goldsmith, S.P. Virostek, S.A. Finnegan, Impact on ceramic targets, J. Appl. Mech. Trans. ASME. 54 (1987) 373–378. doi:10.1115/1.3173022.

[10] R.L. Woodward, A Basis for Modelling Ceramic Composite Armour Defeat (AR 005-713), Ascot Vale, 1989.

[11] R.L. Woodward, A simple one-dimensional approach to modelling ceramic composite armour defeat, Int. J. Impact Eng. 9 (1990) 455–474. doi:10.1016/0734-743X(90)90035-T.

[12] P.C. den Reijer, Impact on ceramic faced armour (Doctoral dissertation), Delft University of Technology, 1991.

[13] J.G. Hetherington, B.P. Rajagopalan, An investigation into the energy absorbed

during ballistic perforation of composite armours, Int. J. Impact Eng. 11 (1991) 33–40. doi:10.1016/0734-743X(91)90029-F.

[14] J.G. Hetherington, The optimization of two component composite armours, Int. J. Impact Eng. 12 (1992) 409–414. doi:10.1016/0734-743X(92)90145-J.

[15] B. Wang, G. Lu, On the optimisation of two-component plates against ballistic impact, J. Mater. Process. Technol. 57 (1996) 141–145. doi:10.1016/0924-0136(95)02050-0.

[16] R. Zaera, V. Sánchez-Gálvez, Analytical modelling of normal and oblique ballistic impact on ceramic/metal lightweight armours, Int. J. Impact Eng. 21 (1998) 133–148. doi:10.1016/S0734-743X(97)00035-3.

[17] I.S. Chocron Benloulo, V. Sánchez-Gálvez, A new analytical model to simulate impact onto ceramic/composite armors, Int. J. Impact Eng. 21 (1998) 461–471. doi:10.1016/S0734-743X(98)00006-2.

[18] G. Ben-Dor, A. Dubinsky, T. Elperin, Optimization of two-component composite armor against ballistic impact, Compos. Struct. 69 (2005) 89–94. doi:10.1016/j.compstruct.2004.05.014.

[19] G. Ben-Dor, A. Dubinsky, T. Elperin, Improved Florence model and optimization of two-component armor against single impact or two impacts, Compos. Struct. 88 (2009) 158–165. doi:10.1016/j.compstruct.2008.02.015.

[20] R. Chi, A. Serjouei, I. Sridhar, G.E.B. Tan, Ballistic impact on bi-layer alumina/aluminium armor: A semi-analytical approach, Int. J. Impact Eng. 52 (2013) 37–46. doi:10.1016/j.ijimpeng.2012.10.001.

[21] A. Serjouei, R. Chi, I. Sridhar, G.E.B. Tan, Empirical Ballistic Limit Velocity Model for Bi-Layer Ceramic–Metal Armor, Int. J. Prot. Struct. 6 (2015) 509–527. doi:10.1260/2041-4196.6.3.509.

[22] A. Serjouei, R. Chi, Z. Zhang, I. Sridhar, Experimental validation of BLV model on bi-layer ceramic-metal armor, Int. J. Impact Eng. 77 (2015) 30–41. doi:10.1016/j.ijimpeng.2014.11.001.

[23] R.T. Tang, H.M. Wen, Predicting the perforation of ceramic-faced light armors subjected to projectile impact, Int. J. Impact Eng. 102 (2017) 55–61. doi:10.1016/j.ijimpeng.2016.11.008.

[24] M. Shaker, H. Abou-Elela, A. Riad, A. Fayed, Numerical investigation of a high-speed projectile penetration into bi-layered lightweight targets, in: 15th Int. Conf. Appl. Mech. Mech. Eng., Military Technical College Kobry El-Kobbah, Cairo, Egypt, 2021.

[25] P.M. Cunniff, Dimensionless parameters for optimization of textile-based body armor systems, in: Proc. 18th Int. Symp. Ballist., 1999: pp. 1303–1310.

[26] Z. Guo, W. Chen, First-Order Approximations of Dynamic Material Strengths for the Ballistic Perforation of Aluminum Target Plates, J. Dyn. Behav. Mater. (2021). doi:10.1007/s40870-021-00304-9.

[27] Z. Guo, W. Chen, Dimensionless parameters for the perforation of ductile plates by armor-piercing rounds, Int. J. Impact Eng. 156 (2021) 103952. doi:10.1016/j.ijimpeng.2021.103952.

[28] A. Tate, A theory for the deceleration of long rods after impact, J. Mech. Phys. Solids. 15 (1967).

[29] Z. Rosenberg, On the relation between the Hugoniot elastic limit and the yield strength of brittle materials, J. Appl. Phys. 74 (1993) 752–753. doi:10.1063/1.355247.

[30] S. Bavdekar, G. Parsard, G. Subhash, S. Satapathy, An improved dynamic expanding cavity model for high-pressure and high-strain rate response of ceramics, Int. J.

Solids Struct. 125 (2017) 77–88. doi:10.1016/j.ijsolstr.2017.07.014.
[31] T.J. Holmquist, A.M. Rajendran, D.W. Templeton, K.D. Bishnoi, A Ceramic Armor Material Database (TR 13754), 1999.
[32] M. Lee, Y.H. Yoo, Analysis of ceramic/metal armour systems, Int. J. Impact Eng. 25 (2001) 819–829. doi:10.1016/S0734-743X(01)00025-2.
[33] S.M. Walley, Historical review of high strain rate and shock properties of ceramics relevant to their application in armour, Adv. Appl. Ceram. 109 (2010) 446–466. doi:10.1179/174367609X422180.
[34] Z. Rozenberg, Y. Yeshurun, The relation between ballastic efficiency and compressive strength of ceramic tiles, Int. J. Impact Eng. 7 (1988) 357–362. doi:10.1016/0734-743X(88)90035-8.
[35] Z. Rosenberg, S. Bless, Y. Yeshurun, K. Okajima, A new definition of ballistic efficiency of brittle materials based on the use of thick-walled backing plates, in: Proc. Int. Conf. Impact Load. Dyn. Behav. Mater., Bremen, 1987: pp. 491–496.
[36] Zvi, Rosenberg, Erez, Dekel, Terminal Ballistics, in: Termin. Ballist., Springer Berlin Heidelberg, 2012: p. 336. doi:10.1007/978-3-642-25305-8.
[37] B. Klein, N. Frage, E. Zaretsky, M.P. Dariel, Dynamic Response of Titanium Carbide-Steel, Ceramic-Metal Composites, in: AIP Conf. Proc., AIP, 2002: pp. 1119–1122. doi:10.1063/1.1483734.

Appendix A: Additional datasets

Conical-nosed projectiles impacting alumina/Al5083 targets (Lee & Yoo)

Lee & Yoo [32] tested a relatively small dataset for alumina/5083 aluminum alloy plates, focusing on the effects of the alumina/aluminum thickness ratio on the ballistic limit velocity of the overall system. Material data and dimensions were largely unreported, and so most of the parameters reported in this section were either inferred or calculated using reported values. Steel projectiles had diameters $D = 12.5$ mm and mass $m_p = 40.7$ g. The nose shape was not specified, but presumed to be sharp, conical-nosed projectiles, as stated in a subsequent study by Tang & Wen [23].

The frontal ceramic material was alumina, with density $\rho_1 = 3380$ kg/m^3. The density indicates that the alumina was likely 85% purity, and so the Hugoniot elastic limit was assumed to be 6.0 GPa (as per Wilkins). Since all the target plates would be scaled by the same strength value, the actual σ_{HEL} value in this case is not especially critical. Alumina plate thicknesses were much thicker than the other studies, with h_1 ranging between 9–25 mm. Aluminum alloy 5083 (temper not specified) was used as backing material, with plate thicknesses h_2 between 6–25 mm. The actual plate dimensions were not reported by Lee & Yoo, but approximate plate thicknesses were solved for using a system of simultaneous equations with constant total areal density as a constraint. Based on calculations, the total areal density of the target system ranges between 90–100 kg/m^2, with deviations likely resulting from under-reporting of material data. The collapsed data points fall broadly along a cubic curve (Figure A2).

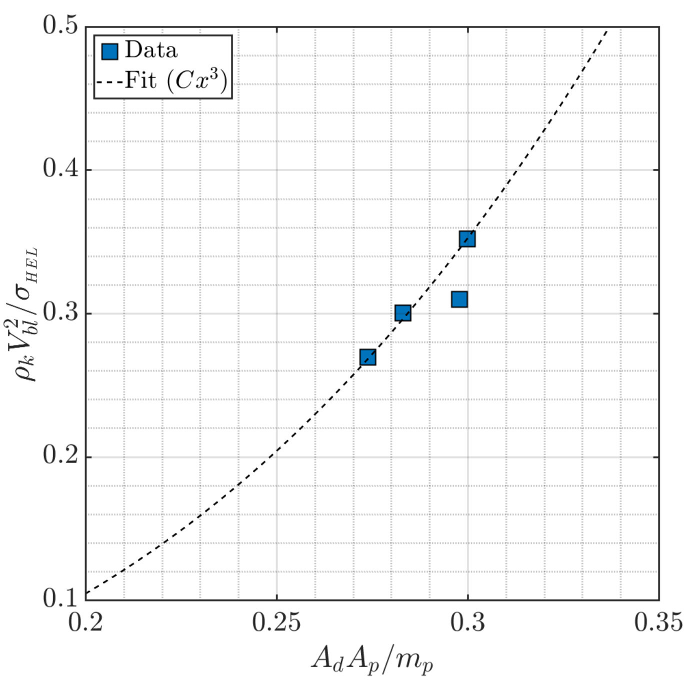

Figure A2: 12.5-mm conical-nosed steel projectiles impacting AD85/Al5083 targets. Fit parameters $C = 13.05$, $R^2 = 0.944$.

Appendix B: Raw ballistic limit data

Table B1: Raw ballistic data for AD85/Al6061-T6 (Dataset W1).

D_p [mm]	m_p [g]	Front	σ_{HEL} [GPa]	ρ_1 [kg/m^3]	h_1 [mm]	Rear	ρ_2 [kg/m^3]	h_2 [mm]	V_{bl} [m/s]
7.62	8.32	AD85	6.0	3430	3.18	Al6061-T6	2765	6.35	405
7.62	8.32	AD85	6.0	3430	4.06	Al6061-T6	2765	3.18	275
7.62	8.32	AD85	6.0	3430	4.06	Al6061-T6	2765	4.95	400
7.62	8.32	AD85	6.0	3430	4.06	Al6061-T6	2765	6.35	490
7.62	8.32	AD85	6.0	3430	4.06	Al6061-T6	2765	7.16	510
7.62	8.32	AD85	6.0	3430	4.06	Al6061-T6	2765	7.57	520
7.62	8.32	AD85	6.0	3430	4.06	Al6061-T6	2765	9.40	580
7.62	8.32	AD85	6.0	3430	5.33	Al6061-T6	2765	6.35	565
7.62	8.32	AD85	6.0	3430	6.35	Al6061-T6	2765	3.18	425
7.62	8.32	AD85	6.0	3430	6.35	Al6061-T6	2765	4.95	535
7.62	8.32	AD85	6.0	3430	6.35	Al6061-T6	2765	6.35	645
7.62	8.32	AD85	6.0	3430	6.35	Al6061-T6	2765	7.09	675
7.62	8.32	AD85	6.0	3430	6.35	Al6061-T6	2765	9.40	755
7.62	8.32	AD85	6.0	3430	7.87	Al6061-T6	2765	3.18	525
7.62	8.32	AD85	6.0	3430	7.87	Al6061-T6	2765	4.52	615
7.62	8.32	AD85	6.0	3430	7.87	Al6061-T6	2765	5.66	690
7.62	8.32	AD85	6.0	3430	7.87	Al6061-T6	2765	6.35	790
7.62	8.32	AD85	6.0	3430	7.87	Al6061-T6	2765	7.72	845
7.62	8.32	AD85	6.0	3430	7.87	Al6061-T6	2765	9.40	910
7.62	8.32	AD85	6.0	3430	8.13	Al6061-T6	2765	6.35	810
7.62	8.32	AD85	6.0	3430	8.13	Al6061-T6	2765	6.35	730
7.62	8.32	AD85	6.0	3430	8.64	Al6061-T6	2765	3.18	545
7.62	8.32	AD85	6.0	3430	8.64	Al6061-T6	2765	4.95	705
7.62	8.32	AD85	6.0	3430	8.64	Al6061-T6	2765	5.74	855
7.62	8.32	AD85	6.0	3430	8.64	Al6061-T6	2765	6.35	870
7.62	8.32	AD85	6.0	3430	8.64	Al6061-T6	2765	6.35	825
7.62	8.32	AD85	6.0	3430	8.64	Al6061-T6	2765	6.35	905
7.62	8.32	AD85	6.0	3430	8.64	Al6061-T6	2765	6.35	775
7.62	8.32	AD85	6.0	3430	8.64	Al6061-T6	2765	7.09	915
7.62	8.32	AD85	6.0	3430	8.64	Al6061-T6	2765	8.43	960
7.62	8.32	AD85	6.0	3430	8.64	Al6061-T6	2765	9.40	990
6.35	4.70	AD85	6.0	3430	7.19	Al6061-T6	2765	5.33	887
7.62	8.12	AD85	6.0	3430	8.64	Al6061-T6	2765	6.35	869
11.43	27.58	AD85	6.0	3430	8.64	Al6061-T6	2765	9.53	588
7.62	8.12	AD85	6.0	3430	5.77	Al6061-T6	2765	6.35	579
11.43	27.58	AD85	6.0	3430	6.35	Al6061-T6	2765	9.53	488
7.62	8.12	AD85	6.0	3430	4.24	Al6061-T6	2765	6.35	488
11.43	27.58	AD85	6.0	3430	5.33	Al6061-T6	2765	9.53	412
7.62	8.12	AD85	6.0	3430	3.56	Al6061-T6	2765	6.35	427
7.62	8.32	AD85	6.0	3430	4.01	-	-	-	80
7.62	8.32	AD85	6.0	3430	6.35	-	-	-	237
7.62	8.32	AD85	6.0	3430	7.81	-	-	-	326
7.62	8.32	AD85	6.0	3430	8.64	-	-	-	335

Table B2: Raw ballistic data for B_4C/Al6061-T6 (Dataset W2).

D_p	m_p	Front	σ_{HEL}	ρ_1	h_1	Rear	ρ_2	h_2	V_{bl}

[mm]	[g]		[GPa]	[kg/m³]	[mm]		[kg/m³]	[mm]	[m/s]
7.62	8.32	B_4C	15.0	2500	3.18	Al6061-T6	2765	6.35	405
7.62	8.32	B_4C	15.0	2500	4.06	Al6061-T6	2765	3.18	275
7.62	8.32	B_4C	15.0	2500	4.06	Al6061-T6	2765	4.95	400
7.62	8.32	B_4C	15.0	2500	4.06	Al6061-T6	2765	6.35	490
7.62	8.32	B_4C	15.0	2500	4.06	Al6061-T6	2765	7.16	510
7.62	8.32	B_4C	15.0	2500	4.06	Al6061-T6	2765	7.57	520
7.62	8.32	B_4C	15.0	2500	4.06	Al6061-T6	2765	9.40	580
7.62	8.32	B_4C	15.0	2500	5.33	Al6061-T6	2765	6.35	565
7.62	8.32	B_4C	15.0	2500	6.35	Al6061-T6	2765	3.18	425
7.62	8.32	B_4C	15.0	2500	6.35	Al6061-T6	2765	4.95	535
7.62	8.32	B_4C	15.0	2500	6.35	Al6061-T6	2765	6.35	645
7.62	8.32	B_4C	15.0	2500	6.35	Al6061-T6	2765	7.09	675
7.62	8.32	B_4C	15.0	2500	6.35	Al6061-T6	2765	9.40	755
7.62	8.32	B_4C	15.0	2500	7.87	Al6061-T6	2765	3.18	525

Table B3: Raw ballistic data for AD85/Glass fiber reinforced polymer (Dataset W3).

D_p [mm]	m_p [g]	Front	σ_{HEL} [GPa]	ρ_1 [kg/m³]	h_1 [mm]	Rear	ρ_2 [kg/m³]	h_2 [mm]	V_{bl} [m/s]
7.62	8.32	AD85	6.0	3430	4.06	GFRP	1750	3.18	235
7.62	8.32	AD85	6.0	3430	5.33	GFRP	1750	3.18	338
7.62	8.32	AD85	6.0	3430	4.06	GFRP	1750	6.35	354
7.62	8.32	AD85	6.0	3430	5.33	GFRP	1750	4.45	369
7.62	8.32	AD85	6.0	3430	6.35	GFRP	1750	3.18	469
7.62	8.32	AD85	6.0	3430	5.33	GFRP	1750	6.35	491
7.62	8.32	AD85	6.0	3430	6.35	GFRP	1750	4.45	500
7.62	8.32	AD85	6.0	3430	4.06	GFRP	1750	9.53	512
7.62	8.32	AD85	6.0	3430	5.33	GFRP	1750	7.62	552
7.62	8.32	AD85	6.0	3430	7.87	GFRP	1750	3.18	567
7.62	8.32	AD85	6.0	3430	6.35	GFRP	1750	6.35	582
7.62	8.32	AD85	6.0	3430	7.87	GFRP	1750	4.45	604
7.62	8.32	AD85	6.0	3430	5.33	GFRP	1750	9.53	631
7.62	8.32	AD85	6.0	3430	6.35	GFRP	1750	7.62	671
7.62	8.32	AD85	6.0	3430	8.64	GFRP	1750	3.18	613
7.62	8.32	AD85	6.0	3430	8.64	GFRP	1750	4.45	646
7.62	8.32	AD85	6.0	3430	7.87	GFRP	1750	6.35	728
7.62	8.32	AD85	6.0	3430	6.35	GFRP	1750	9.53	735
7.62	8.32	AD85	6.0	3430	7.87	GFRP	1750	7.62	796
7.62	8.32	AD85	6.0	3430	5.33	GFRP	1750	12.70	716
7.62	8.32	AD85	6.0	3430	8.64	GFRP	1750	6.35	848
7.62	8.32	AD85	6.0	3430	8.64	GFRP	1750	6.35	820
7.62	8.32	AD85	6.0	3430	8.64	GFRP	1750	6.35	850
7.62	8.32	AD85	6.0	3430	8.64	GFRP	1750	6.83	823
7.62	8.32	AD85	6.0	3430	8.64	GFRP	1750	7.62	872
7.62	8.32	AD85	6.0	3430	7.87	GFRP	1750	9.53	832
7.62	8.32	AD85	6.0	3430	6.35	GFRP	1750	12.70	796
7.62	8.32	AD85	6.0	3430	8.64	GFRP	1750	9.53	905
7.62	8.32	AD85	6.0	3430	7.87	GFRP	1750	12.70	899
7.62	8.32	AD85	6.0	3430	8.64	GFRP	1750	12.70	963

Table B4: Raw ballistic data for AD85/various materials (Dataset W4).

D_p [mm]	m_p [g]	Front	σ_{HEL} [GPa]	ρ_1 [kg/m³]	h_1 [mm]	Rear	ρ_2 [kg/m³]	h_2 [mm]	V_{bl} [m/s]

7.62	8.32	AD85	6.0	3430	8.64	6061-T6 aluminum alloy	2700	6.35	869
7.62	8.32	AD85	6.0	3430	8.64	2024-T4 aluminum alloy	2655	6.35	823
7.62	8.32	AD85	6.0	3430	8.64	7079-T6 aluminum alloy	2655	6.35	907
7.62	8.32	AD85	6.0	3430	8.64	Ti-120 VCA	4396	3.18	869
7.62	8.32	AD85	6.0	3430	8.64	Mg-Th alloy	1725	6.35	640
7.62	8.32	AD85	6.0	3430	8.64	Lockalloy	2040	6.35	694
7.62	8.32	AD85	6.0	3430	8.64	TRIP steel	7768	2.29	762
7.62	8.32	AD85	6.0	3430	8.64	1.57-mm Ti-120 VCA/3.18-mm GFRP	2779	4.75	694
7.62	8.32	AD85	6.0	3430	8.64	6.35-mm Be/1.57-mm Ti-120 VCA	2332	7.92	915
7.62	8.32	AD85	6.0	3430	7.87	6.35-mm Be/1.57-mm Ti-120 VCA[a]	2332	7.92	846

[a] Frontal AD85 thickness for this test was 7.87 mm

Table B5: Raw ballistic data for various ceramics/Al6061-T6 (Dataset W5).

D_p [mm]	m_p [g]	Front	σ_{HEL} [GPa]	ρ_1 [kg/m^3]	h_1 [mm]	Rear	ρ_2 [kg/m^3]	h_2 [mm]	V_{bl} [m/s]
7.62	8.32	B_4C (Mat. #202)	15.0	2500	7.37	Al6061-T6	2765	6.35	823
7.62	8.32	BeO	8.50	2840	6.35	Al6061-T6	2765	6.35	762
7.62	8.32	Coors AD85 alumina (Mat. #602)	6.00	3430	8.64	Al6061-T6	2765	6.35	869
7.62	8.32	Coors AD999 alumina (Mat. #705)	8.40[a]	3960	6.35	Al6061-T6	2765	6.35	811
7.62	8.32	WESGO 995 alumina (Mat. #704)	8.40	3850	7.70	Al6061-T6	2765	6.35	875
7.62	8.32	Diamonite alumina	8.00	3720	8.64	Al6061-T6	2765	6.35	966
7.62	8.32	Carborundum h.p. alum. (Mat. #703)	14.0	3920	6.35	Al6061-T6	2765	6.35	777
7.62	8.32	Si	8.50	2330	6.35	Al6061-T6	2765	6.35	366
7.62	8.32	SiC (Mat. #105)	8.00	3090	6.35	Al6061-T6	2765	6.35	663
7.62	8.32	AlB_{12}	9.60	2530	6.35	Al6061-T6	2765	6.35	686
7.62	8.32	Be_2B	6.70	2030	6.35	Al6061-T6	2765	6.35	655
7.62	8.32	TiB_2 (Mat. #302)	5.40	4460	5.99	Al6061-T6	2765	6.35	692
7.62	8.32	$TiBe_{12}$	5.40	2250	6.35	Al6061-T6	2765	6.35	686
7.62	8.32	Pure TiC	5.87[b]	4880	6.35	Al6061-T6	2765	6.35	762

[a] assumed to be same as WESGO 995 alumina
[b] values obtained from Klein et al. [37]

Table B6: Raw ballistic data for AD85/various materials (Dataset M).

D_p [mm]	m_p [g]	Front	σ_{HEL} [GPa]	ρ_1 [kg/m^3]	h_1 [mm]	Rear	ρ_2 [kg/m^3]	h_2 [mm]	V_{bl} [m/s]
12.7	30.0	AD85	6.0	3410	6.35	Kevlar	1200	3.18	116
12.7	30.0	AD85	6.0	3410	6.35	Kevlar	1200	4.75	132
12.7	30.0	AD85	6.0	3410	6.35	Kevlar	1200	6.35	232
12.7	30.0	AD85	6.0	3410	6.35	Kevlar	1200	9.53	281
12.7	30.0	AD85	6.0	3410	6.35	Kevlar	1200	12.70	338
12.7	30.0	AD85	6.0	3410	6.35	Al-2024-O	2780	1.59	113
12.7	30.0	AD85	6.0	3410	6.35	Al-2024-O	2780	3.18	172
12.7	30.0	AD85	6.0	3410	6.35	Al-2024-O	2780	4.75	235
12.7	30.0	AD85	6.0	3410	6.35	Al-2024-O	2780	6.35	285
12.7	30.0	AD85	6.0	3410	6.35	Al-2024-O	2780	9.53	381
12.7	30.0	AD85	6.0	3410	6.35	SAE 1020	7870	1.59	168
12.7	30.0	AD85	6.0	3410	6.35	SAE 1020	7870	2.38	275
12.7	30.0	AD85	6.0	3410	6.35	SAE 1020	7870	3.18	320
12.7	30.0	AD85	6.0	3410	6.35	SAE 1020	7870	6.35	591
12.7	30.0	AD85	6.0	3410	6.35	SAE4130	7850	1.59	201

12.7	30.0	AD85	6.0	3410	6.35	SAE4130	7850	2.40	266
12.7	30.0	AD85	6.0	3410	6.35	SAE4130	7850	3.18	351
12.7	30.0	AD85	6.0	3410	6.35	SAE4130	7850	6.35	657
12.7	30.0	AD85	6.0	3410	3.18	-	-	-	22
12.7	30.0	AD85	6.0	3410	6.35	-	-	-	57
12.7	30.0	AD85	6.0	3410	12.70	-	-	-	103

Table B8: Raw ballistic data for alumina/Al5083 targets (Lee & Yoo) [32].

D_p [mm]	m_p [g]	Front	σ_{HEL} [GPa]	ρ_1 [kg/m^3]	h_1 [mm]	Rear	ρ_2 [kg/m^3]	h_2 [mm]	V_{bl} [m/s]
12.5	40.7	AD85	6.0	3380	9.91	Al5083	2260	25.40	751
12.5	40.7	AD85	6.0	3380	15.05	Al5083	2260	19.05	777
12.5	40.7	AD85	6.0	3380	20.96	Al5083	2260	12.70	824
12.5	40.7	AD85	6.0	3380	25.00	Al5083	2260	6.35	758

Appendix C: Discussion of Rosenberg & Yeshurun's data

In a previous work by Rosenberg & Yeshurun, the ballistic limit velocities for several ceramics were shown to fall on a single curve that decreases with increasing density [34]. For the same ceramic areal density, a less dense ceramic will be thicker and vice versa, and this larger thickness leads to longer dwell times before complete ceramic failure, leading to better ceramic performance. We were unable to find the same experimental data points used by Rosenberg & Yeshurun to demonstrate the inverse relation to the frontal ceramic density.

Nonetheless, we have digitized the data points in their study and back-calculated the respective V_{bl} and ceramic thicknesses h_1, assuming a constant areal density for all ceramic fronts of about 15.88 kg/m^2 (using BeO+B from Table 3 in Wilkins' fourth report [6] as a reference data point).

Table C1: Digitized and back-calculated data from Rosenberg & Yeshurun [34].

Front	σ_{HEL} [GPa]	ρ_1 [kg/m^3]	h_1 [mm]	Rear	ρ_2 [kg/m^3]	h_2 [mm]	V_{bl} [m/s]	Metric
B_4C (Mat. #202)	15.0	2500	6.39	Al6061-T6	2765	6.35	723	1.00
BeO+B	8.50	2840	6.36	Al6061-T6	2765	6.35	724	1.00
AlB_{12}	9.60	2530	6.31	Al6061-T6	2765	6.35	679	0.94
BeO	8.50	2840	5.59	Al6061-T6	2765	6.35	677	0.94
SiC (Mat. #105)	8.00	3090	5.18	Al6061-T6	2765	6.35	543	0.75
Coors AD85 alumina (Mat. #602)	6.00	3430	4.64	Al6061-T6	2765	6.35	470	0.65
Diamonite alumina	8.00	3720	4.29	Al6061-T6	2765	6.35	480	0.66
WESGO 995 alumina (Mat. #704)	8.40	3850	4.12	Al6061-T6	2765	6.35	479	0.66
Carborundum h.p. alum. (Mat. #703)	14.0	3920	4.05	Al6061-T6	2765	6.35	512	0.71
Coors AD999 alumina (Mat. #705)	8.40[a]	3960	3.99	Al6061-T6	2765	6.35	531	0.73
TiB_2 (Mat. #302)	5.40	4460	3.56	Al6061-T6	2765	6.35	405	0.56
Pure TiC	5.87[b]	4880	3.26	Al6061-T6	2765	6.35	399	0.55

Similarly, with the digitized and back-calculated data from Rosenberg, we note that the Hugoniot elastic limit has a strong influence when the ballistic limit is normalized by the frontal areal density (Figure C1), a trend also demonstrated in Table I.

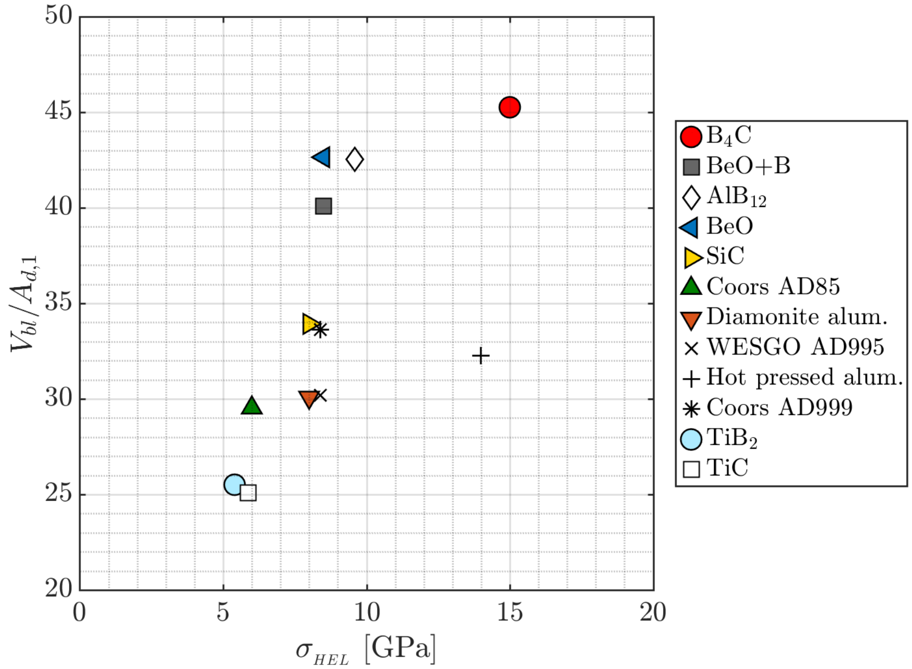

Figure C1: Trend of increasing $V_{bl}/A_{d,1}$ with an increasing Hugoniot elastic limit for digitized data points from Rosenberg & Yeshurun [34].